PHYSICAL REVIEW MATERIALS **1**, 052001(R) (2017)

Nearest-neighbor Kitaev exchange blocked by charge order in electron-doped α-$RuCl_3$

A. Koitzsch,[1] C. Habenicht,[1] E. Müller,[1] M. Knupfer,[1] B. Büchner,[1] S. Kretschmer,[1,2] M. Richter,[1,3] J. van den Brink,[1,3] F. Börrnert,[1,4] D. Nowak,[5] A. Isaeva,[5] and Th. Doert[5]

[1]*IFW-Dresden, Helmholtzstrasse 20, D-01069 Dresden, Germany*

[2]*Helmholtz Zentrum Dresden Rossendorf, Postfach 51 01 19, D-01314 Dresden, Germany*

[3]*Dresden Center for Computational Materials Science (DCMS), D-01062 Dresden, Germany*

[4]*Materialwissenschaftliche Elektronenmikroskopie, Universität Ulm, Albert-Einstein-Allee 11, D-89081 Ulm, Germany*

[5]*Technische Universität Dresden, Department of Chemistry and Food Chemistry, D-01062 Dresden, Germany*

(Received 2 June 2017; published 3 October 2017)

A quantum spin liquid might be realized in α-$RuCl_3$, a honeycomb-lattice magnetic material with substantial spin-orbit coupling. Moreover, α-$RuCl_3$ is a Mott insulator, which implies the possibility that novel exotic phases occur upon doping. Here, we study the electronic structure of this material when intercalated with potassium by photoemission spectroscopy, electron energy loss spectroscopy, and density functional theory calculations. We obtain a stable stoichiometry at $K_{0.5}RuCl_3$. This gives rise to a peculiar charge disproportionation into formally Ru^{2+} ($4d^6$) and Ru^{3+} ($4d^5$). Every Ru $4d^5$ site with one hole in the t_{2g} shell is surrounded by nearest neighbors of $4d^6$ character, where the t_{2g} level is full and magnetically inert. Thus, each type of Ru site forms a triangular lattice, and nearest-neighbor interactions of the original honeycomb are blocked.

DOI: 10.1103/PhysRevMaterials.1.052001

The quantum spin liquid (QSL) is an exotic state of matter that carries fractionalized excitations, completely different from the standard spin waves found for conventional magnetic order [1]. The long search for a realization of this state has recently led to α-$RuCl_3$, a layered honeycomb Mott insulator with a $4d^5$ configuration and substantial spin-orbit coupling [2,3]. From measurements of the magnetic excitation spectrum [3–5], but also from other experiments [6–11] and theory [12–16], evidence is mounting that α-$RuCl_3$ is close to a Kitaev QSL, that is, a realization of the exactly solvable Kitaev model [17], with some modifications due to Heisenberg interactions [6,18–20]. In particular, there are indications of a QSL state in an external magnetic field [21–25]. This offers the opportunity to study the fractionalized excitations, most prominently Majorana fermions, and, possibly, to exploit the fact that they are protected from decoherence for quantum information processing schemes [26].

The magnetic state is usually described within the framework of Heisenberg-Kitaev Hamiltonians. However, these attempts face the difficulty that the exchange parameters are not exactly known, and higher-order interactions (i.e., beyond nearest neighbor) can be decisive [15,27–29]. This problem hinders a deeper understanding and theoretical progress in the field.

The QSL is the main driver of interest in α-$RuCl_3$, but α-$RuCl_3$ is also a Mott insulator. Doping a Mott insulator often results in novel ground states with intriguing properties. Well-known examples are cuprates and manganates. Usually, also the magnetic order associated with the Mott state reacts sensitively to doping. Therefore, doping α-$RuCl_3$ is a promising proposition for both (i) stabilizing new, interesting phases, and (ii) probing the properties of the QSL.

Here, we study the electronic structure of electron-doped α-$RuCl_3$. This is achieved by *in situ* potassium intercalation. An apparent goal of such an approach is to reach a metallic phase. However, this has not been accomplished, similar to previous attempts by rubidium doping instead of potassium [30]. Nevertheless, we show by a combination of electron energy loss spectroscopy (EELS), photoemission spectroscopy (PES), and density functional theory (DFT) that electron doping alters the ground state of α-$RuCl_3$ in a peculiar fashion. We observe a charge disproportionation that quenches the magnetic moment at every alternate Ru site and may serve as a platform to study the interplay of nearest-neighbor and next-nearest-neighbor Kitaev exchange.

Platelet-like single crystals of α-$RuCl_3$ were grown by chemical vapor transport reactions. PES measurements were performed using a laboratory-based system at room temperature after cleaving the crystals *in situ*. The EELS measurements in transmission have been conducted using thin films ($d \approx 100$ nm) at $T = 20$ K. Undoped crystals were intercalated *in situ* by metal vapor from potassium dispensers. The density functional (DF) calculations were performed with the all-electron full-potential local-orbital (FPLO) code [31,32]. See the Supplemental Material for further details [33].

Figure 1(a) shows the effect of successive K intercalation on the low-energy loss function measured by EELS in transmission, a bulk sensitive probe. The pristine spectrum shows a peak at $E = 1.2$ eV (labeled **A**), which corresponds to optical gap excitations. The peaks at higher energies (**B**–**D**) are due to crystal field and charge-transfer excitations [11]. K intercalation causes drastic changes to the electronic structure, in particular to the character of the gap. The inset of Fig. 1(a) expands the low-energy region. We observe that with increasing K content, the spectral weight of the original **A** peak decreases and a new peak at lower energies appears (labeled **a**). Finally, at saturation, **A** completely vanishes. To find a rationale of these observations, we show a schematic picture of the low-energy electronic structure in Fig. 1(b). Near the Fermi energy, the electronic states are dominated by Ru $4d$ character. In the undoped case, **A** corresponds to excitations across the Mott gap ($d^5d^5 \rightarrow d^4d^6$). With doping, new d^6 states are created inside the gap. The fact that **A** completely vanishes in the experiment could be naturally explained by full electron doping, that is, every Ru^{3+} ($4d^5$) ion is reduced

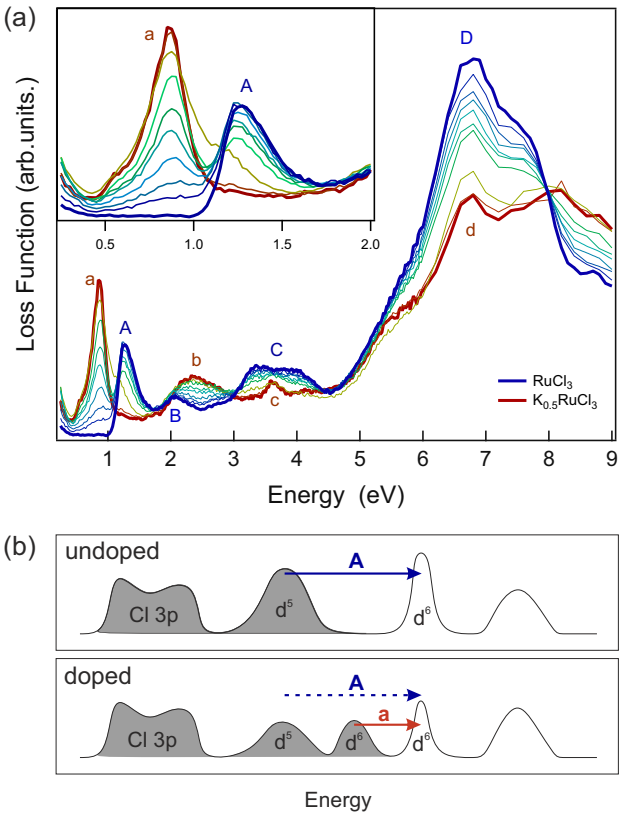

FIG. 1. (a) Loss function measured by electron energy loss spectroscopy for different degrees of potassium intercalation of α-$RuCl_3$ starting from the undoped material and reaching saturation at $K_{0.5}RuCl_3$. Capital letters mark peaks in the spectrum of the undoped material, while small letters mark peaks in the spectrum of the doped material. Inset: magnification of the gap region. (b) Schematic representation of the one-particle low-energy electronic structure of undoped and doped α-$RuCl_3$. Capital and small letters correspond to the peak assignments in (a).

to Ru^{2+} ($4d^6$) by the formation of $KRuCl_3$. Then the occupied d^5 states would disappear. However, this stoichiometry is not realized.

Quantitative x-ray photoemission spectroscopy (XPS), core-level EELS, and DFT consistently hint at a saturated stoichiometry $K_{0.5}RuCl_3$. Further, low-energy electron diffraction (LEED) shows a hexagonal pattern as in the pristine sample with modest lattice expansion but without superstructure (see the Supplemental Material for details). This information allows us to construct a structural model in which the K intercalation takes place between two adjacent Cl layers and occupies interstitial sites (see Fig. 2 and the Supplemental Material for details). Most intriguingly, within our DF calculations a ground state with charge order among the two Ru sites, denoted Ru(1) and Ru(2) henceforth, is found. This charge order is not driven by structural symmetry breaking due to the K intercalation. To show this, we relaxed the same structure, $K_{0.5}RuCl_3$(a), but with exchanged Ru charge and spin states, i.e., starting from the density and d-occupation data of the respective other Ru position (see Fig. 1 in the Supplemental Material). In this way, we obtained a slightly modified geometry, denoted $K_{0.5}RuCl_3$(a′) in Table I of the Supplemental Material. The electronic state remained essentially unchanged, but with Ru(1) and Ru(2) features exchanged. The total energy of the new solution is only 4 meV per formula unit higher than that of the previous one. This means that the slightly different structural environment of Ru(1) and Ru(2) in $K_{0.5}RuCl_3$(a) allows for charge and spin disproportionation due to the broken structural symmetry; however, it does not determine which of the two Ru sites has a hole in the t_{2g} band and which is nonmagnetic. Since the charge order even develops in the case of $K_{0.5}RuCl_3$(b) (see Fig. 1 in the Supplemental Material), where originally both Ru positions are identical, the order is generic for the considered composition, and structural details do not matter.

The Ru $4d$ projected densities of states (DOS) of the isomer from Figs. 2(a) and 2(b) and of prisitine $RuCl_3$ are presented in Figs. 2(c) and 2(d). The calculations support the schematic picture in Fig. 1(b). New states are created inside the Mott gap by potassium doping. The striking difference between $RuCl_3$ and $K_{0.5}RuCl_3$ consists in a splitting of the occupied t_{2g} and of the unoccupied e_g bands in the latter case, caused by the charge order. The empty t_{2g} subband of $RuCl_3$ can be identified as the driving force of the charge order: Upon doping this band to half-filling, it is split into an occupied, Ru(1)-dominated and an unoccupied, Ru(2)-dominated part. Further, the observed reduction of the gap size from $\mathbf{A} = 1.2$ eV in $RuCl_3$ to $\mathbf{a} = 0.8$ eV in $K_{0.5}RuCl_3$ can be understood by the splitting of the occupied t_{2g} band into an upper Ru(1) subband at the Fermi level and a lower Ru(2) subband. The distance of the latter to the first empty Ru(2) band is fixed by the U term.

The described situation is summarized in Figs. 2(e) and 2(f) and explains the complete suppression of **A** upon half-doping. In the undoped case, the gap is defined by the Mott excitation $d^5d^5 \rightarrow d^4d^6$. In the doped case, this transition is blocked, as all d^5 sites are surrounded by d^6 sites. The gap excitation **a** is now associated with the charge fluctuation $d^6d^5 \rightarrow d^5d^6$. Features **B**–**D** of the undoped material have been assigned recently to interband transitions with strong charge-transfer character of **C** and **D** [11] or, alternatively, to d^4d^6 multiplets (**A**–**C**) and charge-transfer excitations (**D**) [34]. While further work is needed for a unified theoretical description, we note that the d^5 initial state concentration still amounts to 50% under full doping and thus it should be present in the doped spectrum but likewise reduced in intensity by 50%. This is indeed observed (see the charge-transfer feature **d** in comparison to **D** in Fig. 1).

Further quantitative support for the calculated charge-ordered ground state is provided by XPS core-level spectra of the Ru $3d$ states; see Fig. 3. The Ru $3d$ line is spin-orbit split into $d_{5/2}$ and $d_{3/2}$ components. With doping, a narrow lower-energy peak appears for both components. Quantitative analysis of these spectra is complicated, and a complete fitting is not possible (see the Supplemental Material). However, we modeled the spectral shape of a high-resolution scan of the fully doped sample (Fig. 3, main panel) by five Voigt peaks (two spin-orbit components for each of the two Ru sites plus one small charge-transfer satellite at the high-energy side) and a standard Shirley background. The intensity ratio of the spin-orbit components is fixed to 3 : 2 and the Ru^{2+} : Ru^{3+} ratio to 1 : 1. Peak positions and total width have been

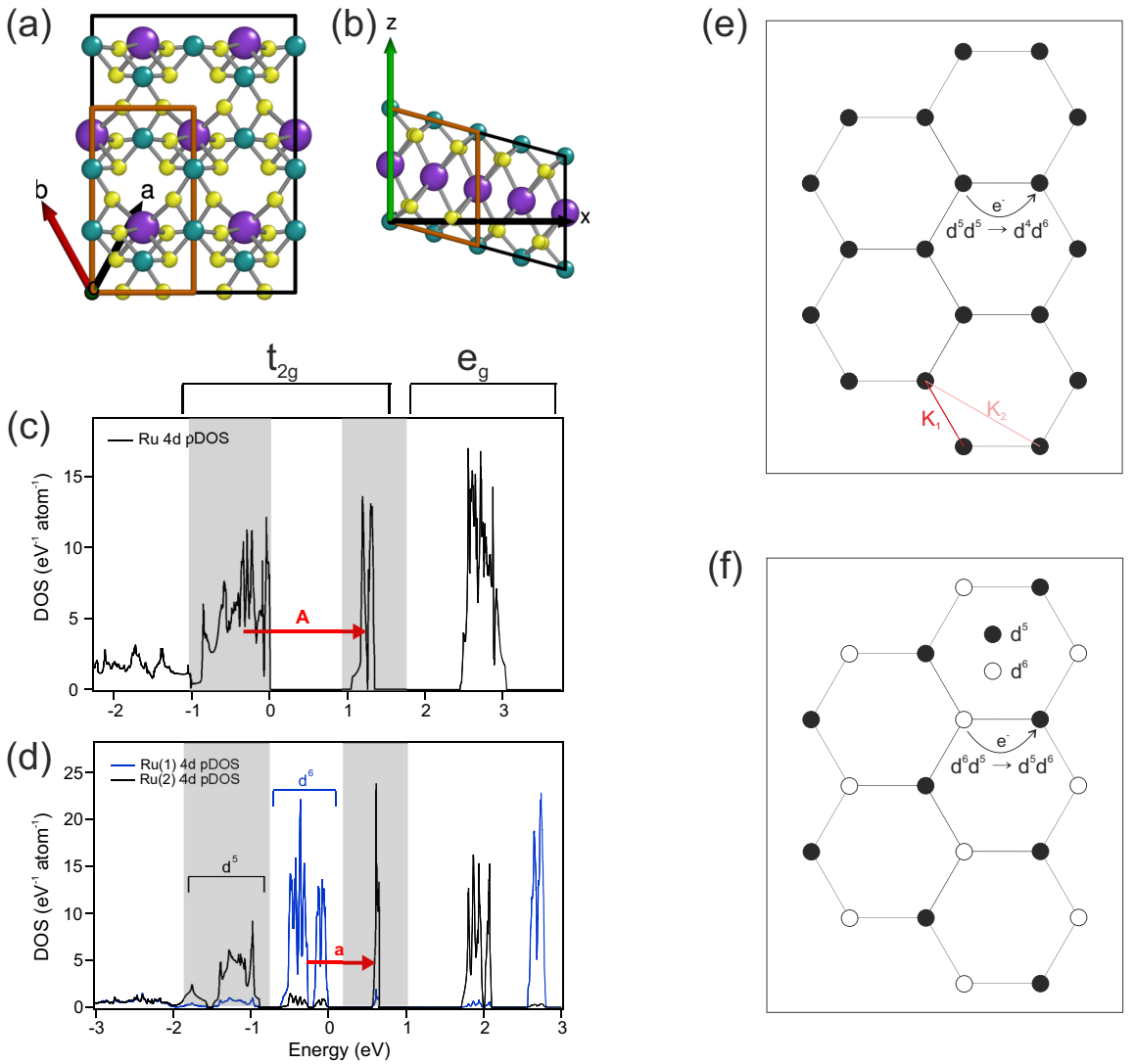

FIG. 2. (a,b) Proposed structure of $K_{0.5}RuCl_3$. The brown frame includes one conventional unit cell (four chemical units). The conventional **b** lattice vector is the sum of the indicated primitive lattice vectors **a** and **b**. (a) View onto the a-b plane. (b) View onto the x-z plane with distinct layers of Ru (green), Cl (yellow), and K (violet). Details of this and of another possible isomer, $K_{0.5}RuCl_3$(b), are given in the Supplemental Material. (c) Densities of states of pristine and (d) K-doped $RuCl_3$ with assignment of the gap feature of related EELS data. The DOS were obtained by means of full relativistic GGA+U calculations in the ferromagnetic state using relaxed structures detailed in the Supplemental Material. Here, both spin channels are added up. Gray shaded areas highlight the lower and upper Hubbard bands of the pristine $RuCl_3$ and how they are inherited to $K_{0.5}RuCl_3$. (e) Honeycomb lattice with d^5 configuration, corresponding to the undoped case. The Mott excitation is sketched. K_1 and K_2 denote nearest- and next-nearest-neighbor Kitaev exchange. (f) Real-space electronic structure of the fully doped $K_{0.5}RuCl_3$.

allowed to vary freely. This fit results in reasonable agreement with experiment, which implicitly confirms a $K_{0.5}RuCl_3$ stoichiometry of the fully doped sample and the Ru^{2+} : Ru^{3+} ratio. The measured energy separation between Ru^{2+} and Ru^{3+} of $\Delta E = 1.8$ eV agrees well with the corresponding DF value of 1.6 eV.

Nominally, K doping of α-$RuCl_3$ to $K_{0.5}RuCl_3$ reduces Ru(1) from Ru^{3+} ($4d^5$) to Ru^{2+} ($4d^6$), while Ru(2) remains in a ($4d^5$) configuration. However, our Mulliken-type analysis tells a different story: the charge difference between Ru(1) and Ru(2) amounts to only 0.15 e, and the K electron is mainly supplied to the Cl ions being adjacent to the K layer. Almost 50% of the Ru $4d$ electrons form a broad hybrid band with Cl $3p$ states between -5.5 and -2.0 eV. Reversely, the narrow t_{2g} and e_g bands contain an appreciable weight of Cl $3p$ between 10% and 60%, i.e., they are formed by $4d$-$3p$ molecular states of the appropriate symmetry (see the Supplemental Material for details). Thus, a better description of the charge-ordered state would be $K^{1+}[RuCl_3]^0[RuCl_3]^{1-}$, where $[RuCl_3]^0$ has one hole in the $4d$-$3p$-t_{2g} states and $[RuCl_3]^{1-}$ has filled $4d$-$3p$-t_{2g} states. Note that each Cl ion is shared among one Ru(1) and one Ru(2), thus all Cl ions carry almost the same charge. For the sake of brevity, we will stick to the nominal notation.

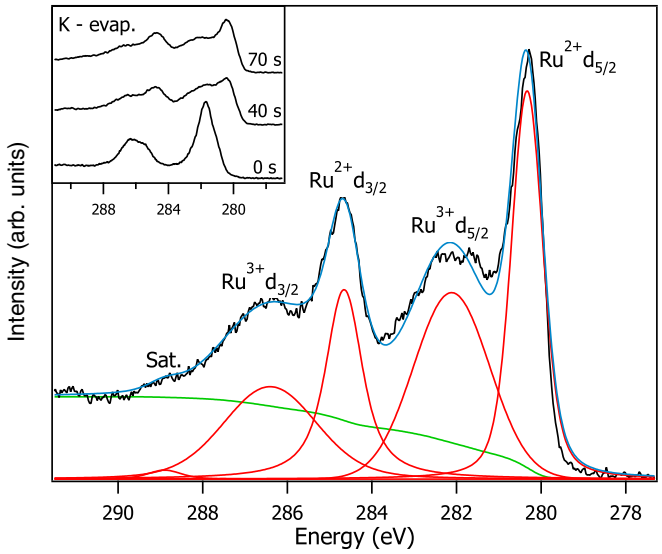

FIG. 3. Ru 3*d* core level measured by x-ray photoemission spectroscopy with model description. Inset: dependence on K evaporation time.

Figure 4 presents the valence-band photoemission results. The doped sample shows an additional peak at low energies [red arrow in Fig. 4(a)]. The original Ru^{3+}-related peak is reduced in intensity and shifts somewhat to higher energies. A similar spectral shape was obtained by Rb intercalation, although without any peak shift [30]. A comparable spectral evolution upon alkali metal doping of the d^1 Mott-insulator TiOCl has been explained previously by the electrostatic potential of the K^+ ions, which effectively localize the doped electron at the closest Ti site [35]. In the present case, at variance, the charge order develops out of a rather homogeneously distributed charge supplied by the K^+ ions to the Cl layers.

With increasing evaporation time, the principal shape of the low-energy region does not change anymore (see the Supplemental Material). For a better comparison of the DF calculations with experiment, we have stretched the energy axis by a renormalization factor of 1.25 and shifted the energy by 0.5 eV within the gap. Such factors are often encountered when comparing photoemission data to DF calculations, especially when the screening is bad [11].

Figure 4(b) shows the angle dependence of the valence band for the doped sample. The Cl 3*p*–related region shows clear dispersion, similar to the undoped sample [11]. This excludes strong surface deterioration by the intercalation process. The Ru 4*d* bands, on the other hand, do not show any dispersion, in agreement with previous results for Rb doping [30], although a small but finite dispersion is present for the undoped material [11]. Within the charge disproportionation scheme this is readily understood: the Ru^{3+} are too far apart in the doped sample to maintain a visible dispersion and so are the newly formed Ru^{2+}. The Cl network is homogeneously doped and retains its dispersion.

The charge-ordered ground state found in the DF calculations is consistent with EELS, valence-band, and core level photoemission data. It is depicted in Fig. 2(f). Other examples of charge order in half-doped Mott insulators are manganites, where the order is of checkerboard type [36,37]. Geometric frustration is present in magnetite (Fe_3O_4) and causes a complicated charge pattern below the Verwey transition [38]. Transition-metal dichalcogenides with similar crystal lattices tend to form charge-density waves [39]. The observed real charge difference in charge-ordered systems is always much smaller than 1 due to the large electrostatic energy cost. Here, our DFT calculation yields a charge difference between Ru(1) and Ru(2) of only 0.15*e*. Nevertheless, the local spin and orbital magnetic moments are distinctly different: $m_s = 0.05\mu_B, m_l = 0.11\mu_B$ for Ru(1); $m_s = 0.73\mu_B, m_l = 0.79\mu_B$ for Ru(2). This means that the charge order causes a difference of one order of magnitude between the magnetic moments of the two Ru sites. The charge order develops due to the combination of two facts: (i) the number of electrons that are available for the $4d$-$3p$-t_{2g} states of each α-$RuCl_3$ entity is not integer, and (ii) a metallic state that would allow us to distribute the extra charge equally among both Ru sites is prevented by the very small dispersion of the bands in the vicinity of the Fermi level. Reduction of U decreases the gap until it is closed below $U = 1$ eV, $J = 0.2$ eV. Concomitantly, the charge order disappears and magnetic moments of comparable size develop at the two Ru positions.

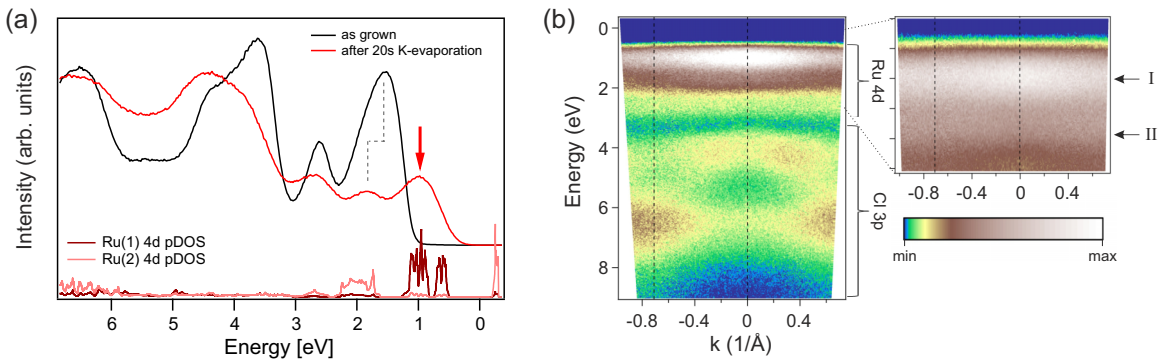

FIG. 4. Valence-band photoemission results. (a) Comparison of undoped and electron-doped α-$RuCl_3$. The arrow marks the new, Ru^{2+} (d^6) -related peak, and the dotted lines highlights the Ru^{3+} states in the doped/undoped sample, respectively. Lower part: Ru 4*d* partial density of states obtained by density functional theory. A stretching factor of 1.25 has been applied to the energy axis of the theory. (b) Angle dependence of the doped valence band and low-energy region.

K intercalation offers a possibility to manipulate the charge and spin pattern of the honeycomb lattice in a controlled fashion. This is especially relevant because these patterns appear independently of the potassium lattice. The effect could be useful to study fundamental properties and to create qualitatively new magnetic ground states. In particular, the zigzag antiferromagnetic order of the parent compound will disappear. The remaining effective triangular d^5 lattice for $K_{0.5}RuCl_3$ is geometrically frustrated. Model calculations are needed to elucidate the magnetic ground state. As the dominating nearest-neighbor Kitaev exchange term vanishes, the prominent background seen in INS [3] and Raman [4] should decrease. Also, the spin-wave spectrum should vanish or, in case an alternative order is established, look different. The suppression of nearest-neighbor Kitaev interactions might allow quantification of higher-order terms, which is a prerequisite for a complete theoretical understanding of the QSL in α-$RuCl_3$. In practice, the process of intercalation modifies bond lengths and, hence, the exchange parameters, which has to be taken into account for a quantitative description. But even on a qualitative level, the originally homogeneous honeycomb lattice of α-$RuCl_3$ decomposes into two triangular lattices of d^5 and d^6 character, which may host new magnetic ground states [15,27]. Recently, in a different approach, the Ru honeycomb lattice has been diluted by Ir substitution, which quickly obstructs the antiferromagnetic order [40].

In summary, we have investigated the electronic structure of potassium-intercalated α-$RuCl_3$. EELS, PES, and DFT show consistently and independently a stable $K_{0.5}RuCl_3$ stoichiometry in which a charge disproportionation into Ru^{2+} and Ru^{3+} takes place. The charge order is accompanied by almost complete quenching of the magnetic moment at every alternate Ru site. This type of combined charge and spin disproportionation on a honeycomb lattice is difficult to achieve otherwise. In principle, double perovskites may have some potential in this direction, but $K_{0.5}RuCl_3$ has the advantage of chemical simplicity. The resulting peculiar state could offer a valuable platform for the investigation of the Kitaev exchange, including higher-order interactions and frustrated magnetism in general.

We thank U. Nitzsche for technical assistance, and R. Ray and H. Rosner for valuable discussions. This work has been supported by the German Research Foundation (DFG) under SFB 1143.

[1] L. Balents, Nature (London) **464**, 199 (2010).
[2] K. W. Plumb, J. P. Clancy, L. J. Sandilands, V. V. Shankar, Y. F. Hu, K. S. Burch, H.-Y. Kee, and Y.-J. Kim, Phys. Rev. B **90**, 041112 (2014).
[3] A. Banerjee, C. A. Bridges, J.-Q. Yan, A. A. Aczel, L. Li, M. B. Stone, G. E. Granroth, M. D. Lumsden, Y. Yiu, J. Knolle, S. Bhattacharjee, D. L. Kovrizhin, R. Moessner, D. A. Tennant, D. G. Mandrus, and S. E. Nagler, Nat. Mater. **15**, 733 (2016).
[4] L. J. Sandilands, Y. Tian, K. W. Plumb, Y.-J. Kim, and K. S. Burch, Phys. Rev. Lett. **114**, 147201 (2015).
[5] A. Banerjee, J. Yan, J. Knolle, C. A. Bridges, M. B. Stone, M. D. Lumsden, D. G. Mandrus, D. A. Tennant, R. Moessner, and S. E. Nagler, Science **356**, 1055 (2017).
[6] M. Majumder, M. Schmidt, H. Rosner, A. A. Tsirlin, H. Yasuoka, and M. Baenitz, Phys. Rev. B **91**, 180401 (2015).
[7] J. A. Sears, M. Songvilay, K. W. Plumb, J. P. Clancy, Y. Qiu, Y. Zhao, D. Parshall, and Y.-J. Kim, Phys. Rev. B **91**, 144420 (2015).
[8] R. D. Johnson, S. C. Williams, A. A. Haghighirad, J. Singleton, V. Zapf, P. Manuel, I. I. Mazin, Y. Li, H. O. Jeschke, R. Valentí, and R. Coldea, Phys. Rev. B **92**, 235119 (2015).
[9] H. B. Cao, A. Banerjee, J.-Q. Yan, C. A. Bridges, M. D. Lumsden, D. G. Mandrus, D. A. Tennant, B. C. Chakoumakos, and S. E. Nagler, Phys. Rev. B **93**, 134423 (2016).
[10] L. J. Sandilands, Y. Tian, A. A. Reijnders, H.-S. Kim, K. W. Plumb, Y.-J. Kim, H.-Y. Kee, and K. S. Burch, Phys. Rev. B **93**, 075144 (2016).
[11] A. Koitzsch, C. Habenicht, E. Müller, M. Knupfer, B. Büchner, H. C. Kandpal, J. van den Brink, D. Nowak, A. Isaeva, and T. Doert, Phys. Rev. Lett. **117**, 126403 (2016).
[12] G. Jackeli and G. Khaliullin, Phys. Rev. Lett. **102**, 017205 (2009).
[13] H.-S. Kim, V. Shankar V., A. Catuneanu, and H.-Y. Kee, Phys. Rev. B **91**, 241110(R) (2015).
[14] J. Chaloupka and G. Khaliullin, Phys. Rev. B **94**, 064435 (2016).
[15] R. Yadav, N. A. Bogdanov, V. M. Katukuri, S. Nishimoto, J. van den Brink, and L. Hozoi, Sci. Rep. **6**, 37925 (2016).
[16] J. Nasu, J. Knolle, D. L. Kovrizhin, Y. Motome, and R. Moessner, Nat. Phys. **12**, 912 (2016).
[17] A. Kitaev, Ann. Phys. (NY) **321**, 2 (2006).
[18] J. Chaloupka, G. Jackeli, and G. Khaliullin, Phys. Rev. Lett. **105**, 027204 (2010).
[19] J. Chaloupka, G. Jackeli, and G. Khaliullin, Phys. Rev. Lett. **110**, 097204 (2013).
[20] Y. Kubota, H. Tanaka, T. Ono, Y. Narumi, and K. Kindo, Phys. Rev. B **91**, 094422 (2015).
[21] S.-H. Baek, S.-H. Do, K.-Y. Choi, Y. S. Kwon, A. U. B. Wolter, S. Nishimoto, J. van den Brink, and B. Büchner, Phys. Rev. Lett. **119**, 037201 (2017).
[22] A. U. B. Wolter, L. T. Corredor, L. Janssen, K. Nenkov, S. Schönecker, S.-H. Do, K.-Y. Choi, R. Albrecht, J. Hunger, T. Doert, M. Vojta, and B. Büchner, Phys. Rev. B **96**, 041405(R) (2017).
[23] R. Hentrich, A. U. B. Wolter, X. Zotos, W. Brenig, D. Nowak, A. Isaeva, T. Doert, A. Banerjee, P. Lampen-Kelley, D. G. Mandrus, S. E. Nagler, J. Sears, Y.-J. Kim, B. Büchner, and C. Hess, arXiv:1703.08623 [cond-mat.str-el].
[24] I. A. Leahy, C. A. Pocs, P. E. Siegfried, D. Graf, S.-H. Do, K.-Y. Choi, B. Normand, and M. Lee, Phys. Rev. Lett. **118**, 187203 (2017).
[25] J. Zheng, K. Ran, T. Li, J. Wang, P. Wang, B. Liu, Z. Liu, B. Normand, J. Wen, and W. Yu, arXiv:1703.08474 [cond-mat.str-el].
[26] A. Kitaev, Ann. Phys. (NY) **303**, 2 (2003).

[27] I. Rousochatzakis, J. Reuther, R. Thomale, S. Rachel, and N. B. Perkins, Phys. Rev. X **5**, 041035 (2015).

[28] S. M. Winter, Y. Li, H. O. Jeschke, and R. Valentí, Phys. Rev. B **93**, 214431 (2016).

[29] Y. Sizyuk, P. Wölfle, and N. B. Perkins, Phys. Rev. B **94**, 085109 (2016).

[30] X. Zhou, H. Li, J. A. Waugh, S. Parham, H.-S. Kim, J. A. Sears, A. Gomes, H.-Y. Kee, Y.-J. Kim, and D. S. Dessau, Phys. Rev. B **94**, 161106 (2016).

[31] K. Koepernik and H. Eschrig, Phys. Rev. B **59**, 1743 (1999).

[32] http://www.FPLO.de.

[33] See Supplemental Material at http://link.aps.org/supplemental/10.1103/PhysRevMaterials.1.052001 for further information on experimental details, technical settings for the calculations, additional DFT results, an extended presentation of experimental EELS and PES results, and for diffraction data.

[34] L. J. Sandilands, C. H. Sohn, H. J. Park, S. Y. Kim, K. W. Kim, J. A. Sears, Y.-J. Kim, and T. W. Noh, Phys. Rev. B **94**, 195156 (2016).

[35] M. Sing, S. Glawion, M. Schlachter, M. R. Scholz, K. Goß, J. Heidler, G. Berner, and R. Claessen, Phys. Rev. Lett. **106**, 056403 (2011).

[36] Y. Tokura and N. Nagaosa, Science **288**, 462 (2000).

[37] E. Dagotto, T. Hotta, and A. Moreo, Phys. Rep. **344**, 1 (2001).

[38] J. P. Wright, J. P. Attfield, and P. G. Radaelli, Phys. Rev. B **66**, 214422 (2002).

[39] K. Rossnagel, J. Phys.: Condens. Matter **23**, 213001 (2011).

[40] P. Lampen-Kelley, A. Banerjee, A. A. Aczel, H. B. Cao, J.-Q. Yan, S. E. Nagler, and D. Mandrus, arXiv:1612.07202 [cond-mat.str-el].